Journal of the Mechanical Behavior of Biomedical Materials 91 (2019) 237–246

Contents lists available at ScienceDirect

Journal of the Mechanical Behavior of Biomedical Materials

journal homepage: www.elsevier.com/locate/jmbbm

Fabrication and selection of surrogate knee implant bearings for experimental evaluation of embedded in-vivo sensors

Robert I. Ponder, Mohsen Safaei, Steven R. Anton*

Dynamic and Smart Systems Laboratory, Tennessee Technological University, Cookeville, TN 38505, USA

ARTICLE INFO

Keywords:
Orthopedic implants
Mechanical behavior
Rapid prototyping
Embedded transducers
Piezoelectric sensing

ABSTRACT

Total Knee Replacement (TKR) is a common procedure that is gaining importance with the aging American population. Although TKR is common, about 20% of patients report being unhappy with their results. Previous research has pointed to misalignment and loosening as contributing factors to negative outcomes. What is lacking in the field of TKR is a sensory system that can determine the internal loads of the knee in a direct manner. Implant bearings embedded with piezoelectric transducers have already shown promise in providing accurate sensing data. To perform further experimentation, prototype implant bearings that can be accurately and efficiently produced are needed. This work investigates various fabrication processes and possible materials to provide a foundation for developing surrogate biomechanical implants, especially those with integrated smart sensors. In this study, an original knee bearing is scanned and the resulting geometries used to generate prototypes. The prototypes are fabricated using a variety of methods including CNC machining and additive manufacturing. The prototypes are then tested to determine load distribution, active sensor performance, as well as kinematic performance under loading. The results of this study show that FDM printing provides quick and affordable results but is not ideal for rigorous experimentation. SLA printed prototypes are improved in final quality with an increase in fabrication time. Lastly, CNC machined processes are more labor intensive but can provide the best material characteristics. The findings from this study aim to have an impact not only on researchers studying biomedical sensing, but on the field of biomechanical implants.

1. Introduction

The human body is not unlike a machine; as it is used and continues to age, parts need to be repaired or replaced to ensure proper function. This causes a high demand for reconstructive procedures such as total knee replacements (TKR). For reference, a schematic showing the components of a TKR is provided in Fig. 1(a). The United States alone has seen a growing demand for TKR as its population continues to age (Dixon, 2004). Despite high numbers of replacements, TKR is a complex procedure and failures are still prevalent (Bozic, 2010). It is estimated that as high as 19% of patients are unsatisfied with their replacement outcome, complaining of discomfort or even failure (Bourne, 2010). Common causes of failure include loosening, infection, and instability of the joint (Sharkey, 2014). In attempt to improve patient outcomes, physicians and researchers have used techniques such as force plates and fluoroscopy to gain an idea of the internal kinetics of the knee joint (Kozanek, 2009). However, these methods can only provide an indirect look at the actual forces occurring inside the joint. To determine these forces in vivo, scientists have developed multiple sensing methods involving modification of the tibial and bearing components. One such method includes using strain gauges embedded into the stem of the tibial component to sense loading (Heinlein, 2007). Other methods include adding pressure sensing matrixes to either the surface or directly below the surface in the polymer bearing (Wasielewski et al., 2004; Manning, 2017). An alternative to these methods that has been shown capable in determining loads is embedding multiple piezoelectric transducers into the polyethylene bearing of the TKR in order to sense load at various locations (see Fig. 1(b) for conceptual sketch) (Safaei et al., 2017). The benefits of using piezoelectric transducers (hereafter referred to as PZTs based on their composition of lead zirconate titanate) include the ability to determine load magnitude and location as well as performing other functions simultaneously such as energy harvesting and/or structural health monitoring (Chen, 2007).

To advance the development of a PZT embedded TKR, further experimental testing need to be performed. However, it is impractical as well as cost prohibitive to embed PZTs into real TKR bearings for experimental purposes due to proprietary designs and limited access to TKR hardware by a general research audience. As a result, it is

* Corresponding author.
E-mail addresses: riponder42@students.tntech.edu (R.I. Ponder), msafaeimo42@students.tntech.edu (M. Safaei), santon@tntech.edu (S.R. Anton).

https://doi.org/10.1016/j.jmbbm.2018.12.018
Received 30 May 2018; Received in revised form 13 December 2018; Accepted 16 December 2018
Available online 18 December 2018

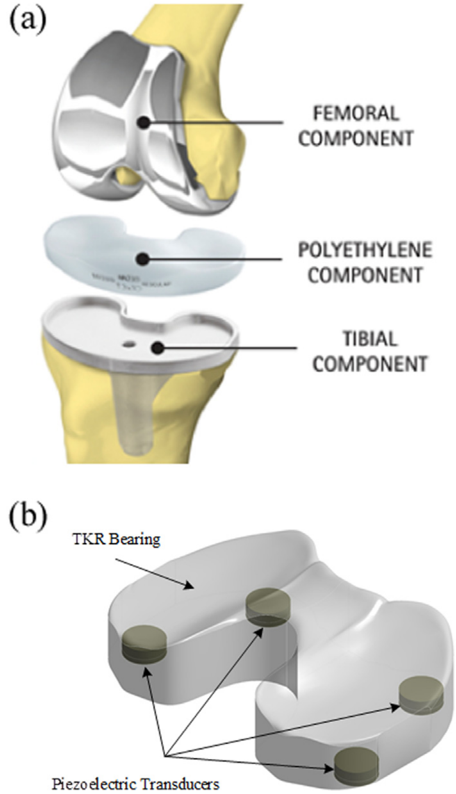

Fig. 1. (a) The major components of a TKR (Safaei et al., 2018a), (b) conceptual sketch of TKR bearing instrumented with multiple PZT transducers (Safaei et al., 2018b).

necessary to develop surrogates which emulate the geometric and material characteristics of the bearing as closely as possible while still being cost effective and time efficient. Previous studies have addressed similar prototypes, evaluating the kinematic performance of replica implants (Verjans et al., 2016). However, these studies did not specifically target the performance of prototypes containing embedded sensors. The aim of this study is to address this need for effective prototypes with embedded transducers.

Since the geometries of TKRs are often proprietary knowledge, 3D scanning technology is used in this work to create a geometric template from which the replicas are produced (Sansoni et al., 2009). From these geometries, prototypes can be produced using various fabrication processes and materials. Modern manufacturing methods provide a variety of choices for developing the bearing replicas. Three processes are investigated in this work that show promise in developing fast yet accurate prototypes within typical university equipment constraints; these include two additive manufacturing processes as well as computer numerical control (CNC) machining. Additive manufacturing has been used successfully for various biomedical applications (Gross, 2014). These have included reconstructive mechanical implants for maxillofacial applications (Saijo, 2009). 3D printed medical implants have even been tested with embedded sensor systems for non-orthopedic functions (Mannoor, 2013). Additionally, metal additive manufacturing has been used to prototype the femoral component of a TKR (Murr, 2012). As a result, two additive manufacturing processes are investigated in this work: stereolithography (SLA) and fused deposition modeling (FDM). While these processes allow for direct printing of the scanned bearing geometry, the materials available for creating prototypes are somewhat limited. CNC machining is, therefore, used as the third process due to its ability to create prototypes out of non-medical grade Ultra-High Molecular Weight Polyethylene (UHMW); a material very similar to the medical grade version used in the actual implants. Various materials as well as a post processing procedure are chosen for these fabrication methods. In the end, a total of eight unique prototypes are developed for evaluation purposes.

The surrogate prototypes are experimentally evaluated to assess several important characteristics. First, the Rockwell hardness of each fabricated material is determined. Then, an experiment is performed that attempts to simulate the dynamic load conditions of normal walking gate to measure three additional characteristics. The first characteristic involves measuring load distribution between the true femoral component and the replica bearing. This is achieved using pressure sensitive films and image processing. The second characteristic involves recording generated voltage data from PZTs embedded in the replica bearing components. For this study, four PZTs are used since this configuration has previously been shown to be capable of sensing the center of pressure for a given applied load (the PZT locations are kept constant and are chosen based on the previous research)(Safaei and Anton, 2017.). The final metric, used to evaluate the kinematic behavior of these prototypes, is displacement as determined by the axial translation of the femoral component during loading. In this work, a benchmark prototype is chosen for its similarity to the true knee bearing. The performance of all other bearing prototypes is experimentally compared to the performance of this benchmark prototype. The benchmark is selected as the CNC polished prototype made from non-medical grade UHMW.

The goal of this study is to show how various replication methods can affect the in vitro experimental performance of an embedded sensory system and bearing. This comparison is made across multiple manufacturing techniques and materials. The overarching goal is to determine which method produces the desired performance for a given parameter, be it voltage output, load distribution, or displacement. This work, therefore, provides a platform for the use of replica prototypes in future work. Further, this information will prove useful not only for experimentation on TKR, but also for experimentation performed on other orthopedic arthroplasties, both with and without embedded sensors.

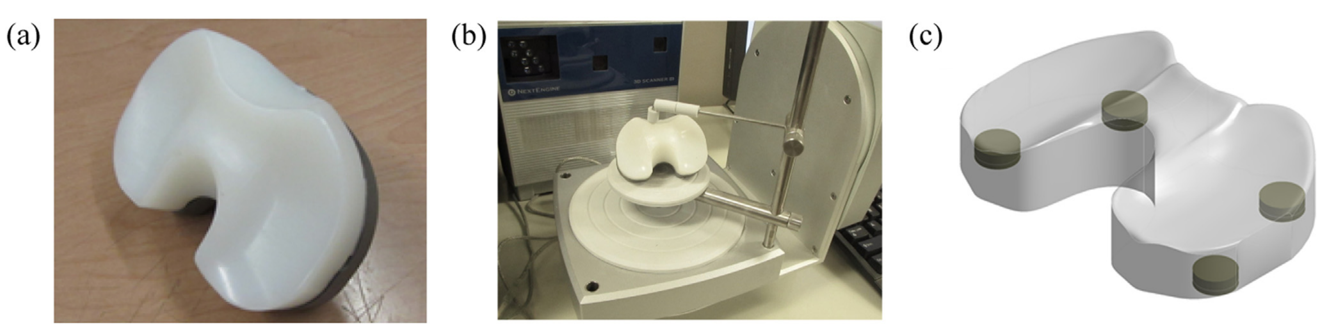

Fig. 2. (a) Original real TKR bearing, (b) 3D scanning the real bearing, (c) final 3D CAD geometry with four embedded PZTs.

2. Methodology

2.1. 3D computer modeling

To produce accurate geometries for the replica bearings, 3D laser scanning is first performed on a real TKR bearing, shown in Fig. 2(a), using a NextEngine Desktop 3D Scanner (NextEngine, Inc), shown in Fig. 2(b). This scanner functions by sweeping multiple lasers across a presented face of the knee bearing. Multiple scans must be produced to capture all of the surfaces of the knee bearing. These individual scans are combined in the complementary NextEngine software to create a 3D geometry. The output of this compilation is an STL file which can be imported to a 3D modeling software, such as SolidWorks, to be parametrized. While in SolidWorks, pockets of size 8.5 mm diameter and 2 mm depth are created at the four predetermined locations, and PZT transducers are embedded inside the bearing (Fig. 2(c)). These files can later be used for 3D printing or CNC machining processes as well as finite element modeling.

2.2. Fabrication

As mentioned in the introduction, eight different prototypes are produced using three different manufacturing processes and a variety of materials. CNC machining is selected due to its standing as a well-known and verified fabrication method, as well as its ability to create parts from solid blocks of material. This allows the use of UHMW which is very similar to the material used in the real bearing component. Additionally, SLA 3D printing is selected which uses lasers along with photoreactive materials to print high quality parts. Finally, FDM 3D printing is selected for its quick and cost effective manufacturing. For processes that were determined to provide a low-quality surface finish, two prototypes were made: one that has no post processing performed, and one that undergoes polishing using 300 grit sandpaper. This polishing is intended to remove features, such as surface roughness, caused by fabrication. A complete list of all fabricated prototypes along with their material properties is provided in Table 1.

A ShopBot desktop router (ShopBot Tools, Inc.) is used to create the CNC prototypes. Prototypes are cut from 2 × 3 × 3 in. blocks of non-medical grade UHMW. A 1/8th inch tapered ball-nosed end mill is used for machining. To provide a quality product, three separate toolpaths are used. The G-code for the toolpaths is generated using PathWorks (ShopBot Tools, Inc). To produce the best contours, the stepover is kept to 9% of the tool diameter for the first toolpath and 5% for the second. The bottom side of the knee bearing is manually machined to create a flat surface with a tolerance of 0.005 in. To create the pockets for the PZTs, an 8.5 mm end mill is plunged 2.5 mm into the base of the bearing replica at the four predetermined locations. The resulting benchmark prototype (polished CNC from UHMW) with attached leads is shown in Fig. 3(a)-(b) and also in Fig. 3(c) i, and the unpolished CNC prototype is shown in Fig. 3(c) ii.

Table 1
Surrogate processes and materials selected.

Surrogate Process	Material	Material Modulus of Elasticity (GPa)	Yield Strength (MPa)
CNC Machined (polished)	UHMW	0.80	40.0
CNC Machined	UHMW	0.80	40.0
FDM (polished)	PLA	3.5	56.6
FDM	PLA	3.5	56.6
FDM (polished)	*t*-glase	0.58	30.8
FDM	*t*-glase	0.58	30.8
SLA	Formlabs Durable	1.26	31.8
SLA	Formlabs Tough	2.7	55.7

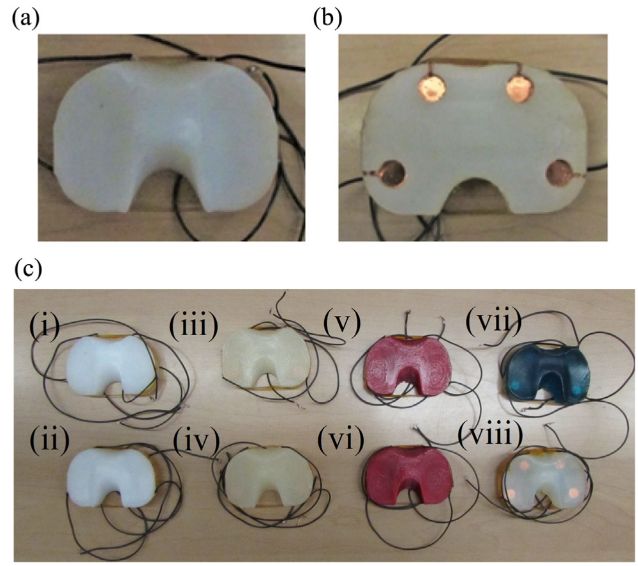

Fig. 3. Polished CNC machined prototype (benchmark) close-up from (a) top and (b) bottom. (c) Prototypes created from all processes including (i) polished CNC machined, (ii) unpolished CNC machined, (iii) PLA unpolished, (iv) PLA polished, (v) t-glase unpolished, (vi) t-glase polished, (vii) SLA Tough, and (viii) SLA Durable.

An adequate investigation of rapid prototyping should include the ubiquitous FDM printing process. Two materials are investigated, both in a polished and unpolished form. Esun PLA (Shenzhen Esun Industrial Co., Ltd.) is selected because of the high prevalence of the material in additive manufacturing; these prototypes are shown in Fig. 3(c) iii & iv. Additionally, Taulman t-glase (Taulman3D, LLC) is investigated due to its more similar stiffness to UHMW; these prototypes are shown in Fig. 3(c) v & vi. For this study, all FDM printed components are made using a Lulzbot TAZ 6 printer (Aleph Objects, Inc.). For all prototypes, 100% rectilinear infill is used with layer heights being maintained at 0.1 mm thick. The only exceptions to this are the top and bottom layer shells which are 0.3 mm thick. The PLA is extruded at 205 °C while t-glase is printed at 240 °C. Bed temperature is maintained at 60 °C for all prototypes. Developing ideal pocket geometries in the FDM prototypes is more involved than CNC or SLA fabrication techniques. First, the parts are printed with four 8.5 mm diameter holes of 2 mm thickness. While the parts are printing, the print job is paused just before covering the four pockets with the next layer. Kapton tape is placed over the pockets to prevent material from sagging into the pockets. After the print is complete, an 8.5 mm end mill is used to increase the depth of the holes to 2.5 mm. This milling operation removes the majority of the Kapton tape used to preserve the pockets.

SLA printing, which has only recently been available to non-industrial users, is known widely for its high quality as well as unique material properties. For the SLA printed prototypes, Formlab's Desktop SLA printers are used (Formlabs, Inc.). As shown in Fig. 3(c) vii & viii, two different materials: Formlabs Tough V3 and Durable V2, are used to create two different prototypes. These are selected in order to test materials of different stiffness. The tough material prototype is printed using a Formlabs Form 1 +. A Formlabs Form 2 printer is used to print the Durable material. This choice is made due to equipment availability and has no effect on the fabrication of the prototypes. Both are printed using the Formlabs PreForm software, which specifies the optimal printing orientation. The components are printed with four pockets of 8.5 mm diameter and 2.5 mm depth. Support material is custom designed to not interfere with critical geometries such as the pockets or top surfaces. Geometric resolution is maintained at 0.05 mm. To obtain the material properties specified by Formlabs, following fabrication, the prototypes are first soaked in two isopropyl alcohol baths for 15 min

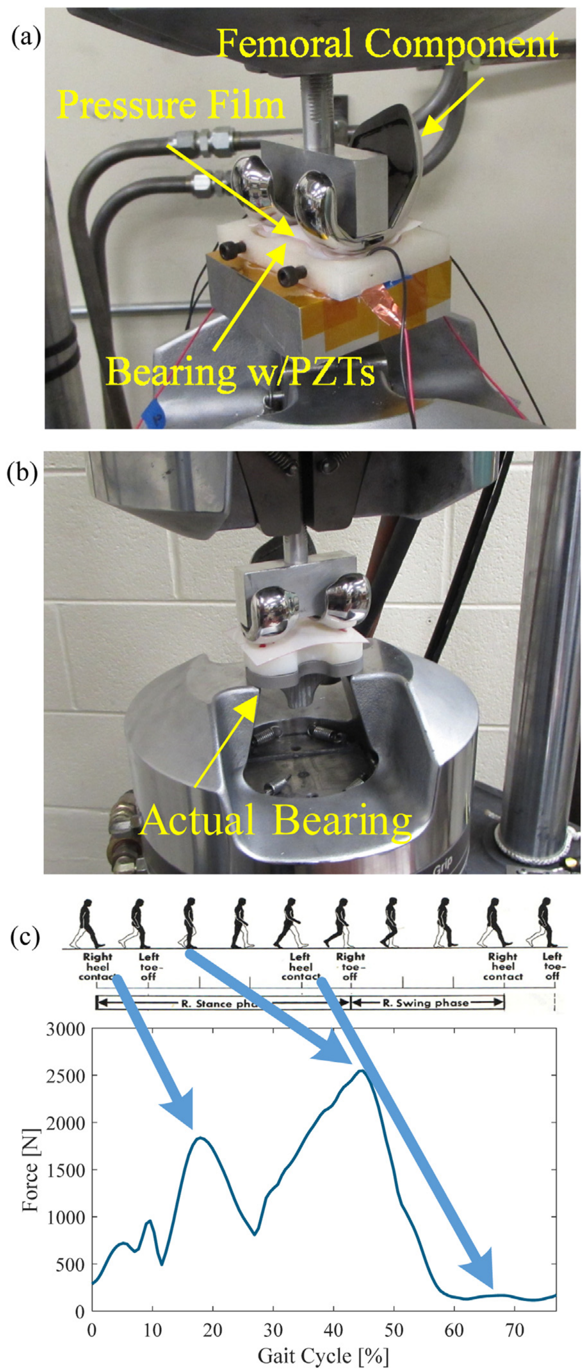

Fig. 4. (a) Load frame with pressure film, femoral component, and instrumented bearing, (b) load frame with pressure film, femoral component, and actual bearing, and (c) load pattern.

each. Next, it is recommended by Formlabs to cure parts in 200 nm wavelength light for one hour. To achieve this, the prototypes are exposed to a black light for one hour while being rotated every 15 min. This ensures an optimal and even cure. Once curing is complete, the support material is removed, and the bottom surface is sanded to remove remaining excess material.

2.3. Experimental setup

As stated before, this study is designed to evaluate four different quantities: Rockwell hardness, load distribution, piezoelectric voltage output, and displacement. Rockwell hardness testing is performed using a Wilson Rockwell Series 2000 tester (Buehler Inc.). The remaining three quantities are measured simultaneously during experimental testing in order to allow correlation between the results. Measurement of these quantities requires simulation of the major loading conditions found inside a knee during normal walking gate. Experimental testing is conducted using an MTS 810 load frame (MTS Systems Corporation), shown in Fig. 4(a). The true femoral component is inserted into the upper clamp of the load frame using a custom aluminum mount. The surrogate bearing component is placed within a frame that rests on a flat compression platen loaded into the lower clamp. The frame is in the shape of the bearing component and uses screws to align and hold the position of the bearing component during testing. This allows for easy replacement of the bearing component while ensuring the position of the bearing during testing remains constant. The overall orientation of the components is designed to replicate the orientation of a true TKR in a standing patient. The load frame utilizes a realistic loading profile that has previously been generated in OpenSim (an open-source biomechanics software) (Wilson et al., 2014).

The Rockwell hardness of the various prototypes is investigated to support the findings of the knee loading experiment, especially the load distribution results. Testing is performed in accordance with the appropriate ASTM standard (ASTM D785-08(2015), 2015). Test samples representing each of the eight prototypes are created. In order to follow testing standards, $4 \times 4 \times 1$ cm^3 blocks are created using the same fabrication processes and post processing. Rockwell Hardness Scale R is used which involves a 10 kg and 60 kg minor and major load in conjunction with a ½ inch ball indentor. Five measurements are taken for each test sample and the mean averages are investigated and compared.

For the measurement of load distribution, pressure sensitive films are placed between the bearing and femoral component while the joint undergoes load (see Fig. 4). After the experiment, the films are scanned and imported into MATLAB where they are overlayed on an image of the knee bearing. This provides a general understanding of the contact patterns and positions. Additionally, the images are imported into ImageJ software (an Open-source Java image processing program developed at the National Institutes of Health) and the contact areas are measured in terms of percentage of the total area of the knee bearing. In addition to determining load distribution of the prototypes, a separate pressure film measurement is taken on an actual knee bearing attached to a tibial tray. This offers the ideal baseline load distribution for comparison.

In order to measure the voltage generation performance, four PZTs are embedded into the prototypes and each placed in parallel with a 1 MΩ load resistor. The voltage outputs of the PZTs are measured across these resistors using an NI 9215 DAQ card along with LabVIEW (National Instruments). Data is later processed using MATLAB. Voltage is recorded at two points during the experiments: once at the beginning during the first few cycles, and then again after the response has reached steady state, which occurs after roughly 10 min or 500 cycles. These are referred to as low cycle and high cycle, respectively, and are designed to investigate any settling that occurs during the experiment. Consideration is given to both the outcomes of individual PZT voltage data as well as total PZT output. The PZTs used in this experiment are APC 850 piezoelectrics (APC International, Ltd.) which are 8 mm in diameter with a 3 mm thickness. These PZTs are specifically chosen to have a greater thickness than the pocket depth of the prototypes, as to ensure all load is transferred to the PZTs.

Displacement data is recorded by the load frame itself. The values recorded represent the axial translation experienced by the femoral component during loading. This translation is representative of the deflection experienced by the bearing component as the metallic platen and femoral component are considered rigid by comparison. This displacement is recorded in the load frame software and later processed using MATLAB to zero the data. As with voltage, displacement is measured both at low cycle and high cycle conditions.

Table 2
Fabrication time and cost analysis.

Process	Fabrication Time (h)	Material Cost (USD per Prototype)
CNC Machining	5	6.75
FDM 3D Printing	6.5	0.62
SLA 3D Printing	10	6.13

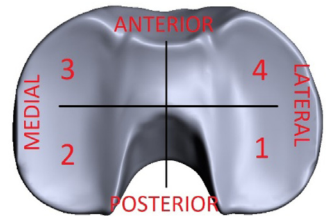

Fig. 5. Coordinate system of bearing component (for a right knee).

3. Results and discussion

3.1. Fabrication analysis

When selecting the best prototype, factors such as fabrication time and cost of materials weigh on the decision of which process to use. Table 2 displays the fabrication time and material cost per part for each method. Fabrication costs outside of materials are not included because it is assumed that access is available to the equipment necessary to complete the process.

Overall, CNC machining has the least amount of fabrication time, meaning new prototypes can be made relatively quickly. That said, 3D printers are usually less labor intensive than CNC machining processes. CNC machines are typically more complex to operate and require supervision while running. Most modern commercial 3D printers, on the other hand, are very user friendly and can be safely left alone without risk. In terms of material cost, FDM printing provides the superior solution by a large margin. These low material costs are mostly because FDM filament is readily available from a variety of vendors. CNC machining always requires buying more material than is volumetrically needed since it is a subtractive process, and SLA resins are specialized photopolymers, thus these processes are more expensive than FDM.

3.2. Surface hardness

Hardness data can be used in conjunction with the load distribution data presented next to help understand the loading behavior of the surrogate implants. Table 3 present the Rockwell hardness data recorded for all of the prototypes investigated. As stated before, results are reported in the Rockwell R scale. In general, the hardness of the prototypes increases with increasing modulus of elasticity, as expected. The exception, however, is that t-glase shows greater respective surface hardness. Overall, the FDM printed prototypes and the SLA Tough prototype displayed higher hardnesses compared to the CNC and SLA Durable prototypes.

3.3. Load distribution

When discussing both load distribution and piezoelectric voltage, it is best to describe the results in terms of the four quadrants of the polymer bearing. This is reasonable as there are four PZTs and, consequently, four load areas to discuss. Fig. 5 displays the layout of the quadrants defined in this work. Additionally, the medical terms for the directions on the face of the bearing are specified. It should be noted that the areas where the femoral component and bearing make contact are often called condyles. Further, area 2 and 3 are in the medial condyle and 1 and 4 are in the lateral condyle.

Pressure sensitive film data was successfully recorded for all eight prototypes as well as the original knee bearing component. The distributions displayed by the films overlaid onto images of the knee bearing are displayed in Fig. 6. Upon visual inspection of the results, it is apparent that softer prototypes such as the CNC UHMW or SLA Durable display larger distributions of load as compared to harder materials such as the FDM printed prototypes and SLA Tough. Additionally, the larger contact surfaces of SLA Durable and the CNC prototypes are more comparable to the real bearing. It should be noted that although t-glase has a relatively low modulus of elasticity, its surface hardness is comparable to that of PLA, likely due to the heating and the extrusion of the FDM printing process. This affects the load distribution, making the load areas of t-glase smaller. This is supported by the hardness results displayed previously which quantitatively show harness comparable to PLA.

Polishing of the CNC and FDM printed prototypes has an obvious visual impact on the load distributions. For the FDM prototypes, the overall contact area is increased as well as more uniform. Processing the images using ImageJ provides a quantitative value for the ratio between contact area between the femoral and bearing component and the total area of the pressure film. The quantitative results for each prototype by contact area percentage relative to the total area of the pressure film are displayed in Table 4. When comparing unpolished samples to polished samples, PLA shows an increase of roughly 63% while t-glase showed closer to 18% increase. The CNC prototype behaved unexpectedly, decreasing by about 29% with polishing. Investigating the individual areas of contact, it can be seen that quadrant 2 increased, while quadrant 4 decreased. This poses the question as to whether polishing changed the geometry of the softer material, causing the load to be redistributed medially and to the posterior. Comparing the two SLA prototypes, Durable has a 65% increase in area as compared to Tough. Visually comparing the load distribution of the real component to the eight prototypes, it is apparent that both SLA and CNC fabricated prototypes provide the most reasonable load distribution. When looking at the individual contact points within the load quadrants for all prototypes, it is apparent that loading favors quadrant 1, with quadrant 3 being the least favored. This was confirmed visually during experimentation where the femoral component tends to contact quadrant 1 before the others.

The main conclusion from the pressure sensitive film data is that polishing lower-quality surfaces, such as FDM printed and CNC machined prototypes, improves surface contact between the condyles of the femoral component and the polymer bearing. Polishing both increases the total area as well as reduces the visible lines (which represent concentrated load), as seen on the pressure films. The CNC machined prototypes raise an interesting question as to how polishing affects softer materials. Load seems to shift from quadrant 4 to quadrant 2 after polishing which may mean a change in geometry of the prototype (Fig. 6(a) and (b)). Future precautions may need to be taken to ensure geometry is preserved, such as a more consistent method of polishing in place of sandpaper. FDM printed parts performed most poorly in surface quality. Due to complex and curved surfaces, it is

Table 3
Averaged hardness results for all prototypes.

CNC UHMW Polished	CNC UHMW Unpolished	FDM PLA Polished	FDM PLA Unpolished	FDM t-glase Polished	FDM t-glase Unpolished	SLA Durable	SLA Tough
45.16	49.84	117.18	110.94	96.56	95.40	77.96	107.44

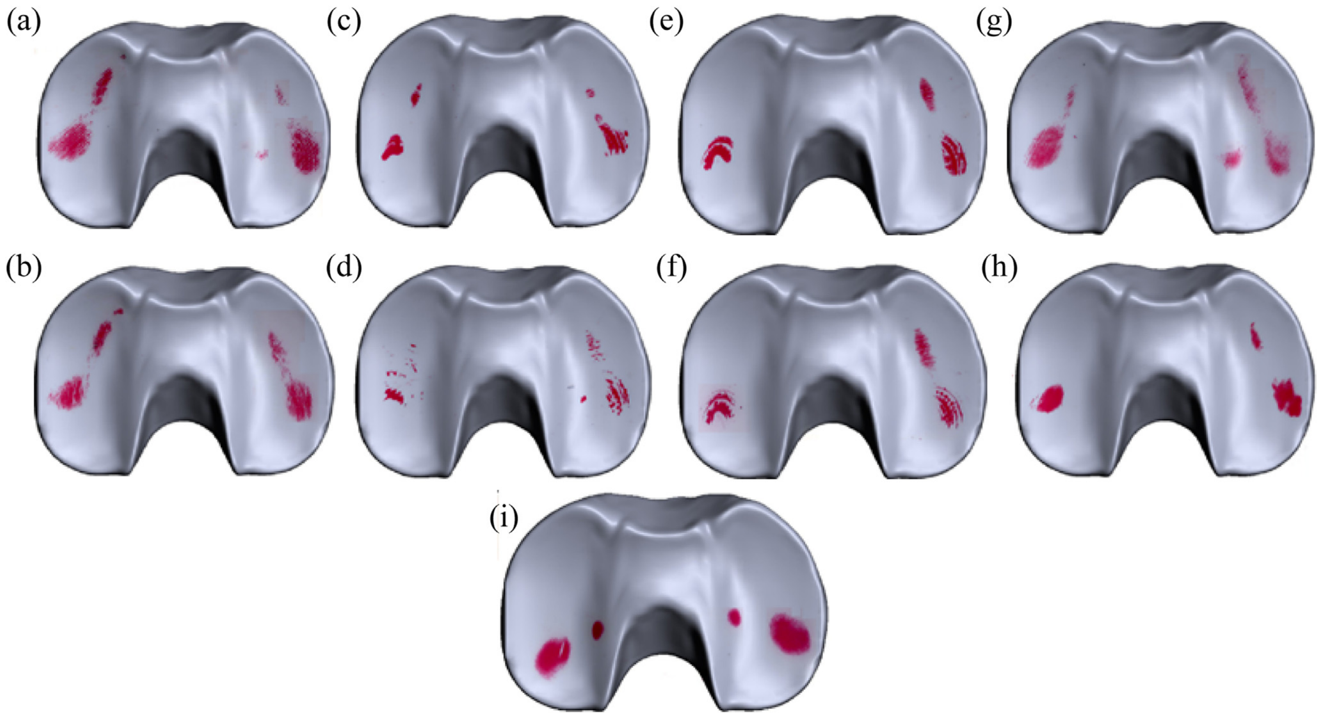

Fig. 6. Load distribution displayed by pressure sensitive films for (a) polished CNC machined (benchmark), (b) non-polished CNC machined, (c) FDM printed PLA, polished, (d) FDM printed PLA, non-polished, (e) FDM printed t-glase, polished, (f) FDM printed t-glase, non-polished, (g) SLA printed Formlabs Durable, (h) SLA printed Formlabs Tough, and (i) original bearing component.

difficult to adequately remove surface roughness caused by the printing process without significantly altering the prototypes. Overall, these results show that SLA printed prototypes perform the best in terms of load distribution, with SLA Durable exhibiting the closest behavior to the real implant in terms of surface area calculated by ImageJ.

3.4. Piezoelectric voltage

Piezoelectric performance is first evaluated by investigating the total voltage generated when summing the output of all four transducers. Recall, data is recorded for low cycle (in the first few loading cycles of the test) and high cycle (after reaching steady state at approximately 10 min of cycling or about 500 cycles) loading conditions. Low cycle voltage results are shown in Fig. 7. For the low cycle data, the generated voltages fall roughly into two groups. The FDM printed prototypes are grouped together and show a peak voltage of around 13 V, whereas the CNC and SLA prototypes are grouped together and show peak voltages of around 5–8 V. Polishing does not seem to cause a significant change in the voltage response of the prototypes.

Voltage responses for the high cycle data are displayed in Fig. 8. Investigating the high cycle data reveals very apparent changes in the voltage performance when compared to the low cycle response. The responses of all the prototypes seem to converge to a peak voltage of around 11 V. These results demonstrate that there is a significant transient response that is resolved with prolonged cycling, possibly due to settling or strain hardening. Note that SLA Durable is slightly lower than the others; however, this is likely due to experimental error.

Investigating the total voltage provides information about overall performance, however, examining the high cycle results for individual PZTs allows for further insight into the load distribution in each prototype. Fig. 9 shows the individual voltages for each of the four PZTs. It should be noted that the PZTs are numbered based upon the quadrant in which the PZT is located (i.e. PZT 1 is placed in quadrant 1, etc.). Upon initial inspection, one can see that PZTs 1 and 2 have higher overall generated voltages compared to PZTs 3 and 4. This is understandable since the femoral contact points, as seen by the pressure sensitive data, are more weighted toward the posterior portion of the knee bearing (Fig. 6). Additionally, the voltages generated by PZT 3 and 4 are more varied between prototypes, owing to the low amount of applied force and resulting generated voltage. Additionally, it should be noted that PZT 2 and 3, which are placed in the medial side of the bearing, display zero generated voltage at various times during the loading cycle as well as overall lower voltages when compared to PZTs 1 and 4, respectively. This suggests that loading favors the lateral portions of the knee implant and that, at times in a loading cycle, there is no loading on the medial side. In summary, PZT 1 generally carries the highest load and thus exhibits the highest generated voltage, while PZT 3 tends to carry the lowest load and exhibits the lowest generated voltage. These findings strongly support the results found via pressure sensitive films which show similar trends.

The voltage results presented here are particularly relevant to the implementation of smart sensors in implantable prototypes. The major discovery of the total sum voltage data is a transient response between early cycling and steady state conditions. This change in response may be due to settling in the overall system as well as strain hardening in the polymer material. Strain hardening has been seen in biomedical

Table 4
Quantitative results of load distribution by percent area of pressure film.

CNC UHMW Polished	CNC UHMW Unpolished	FDM PLA Polished	FDM PLA Unpolished	FDM t-glase Polished	FDM t-glase Unpolished	SLA Durable	SLA Tough	Actual Component
2.042	2.624	1.255	0.769	1.623	1.375	3.070	1.835	2.870

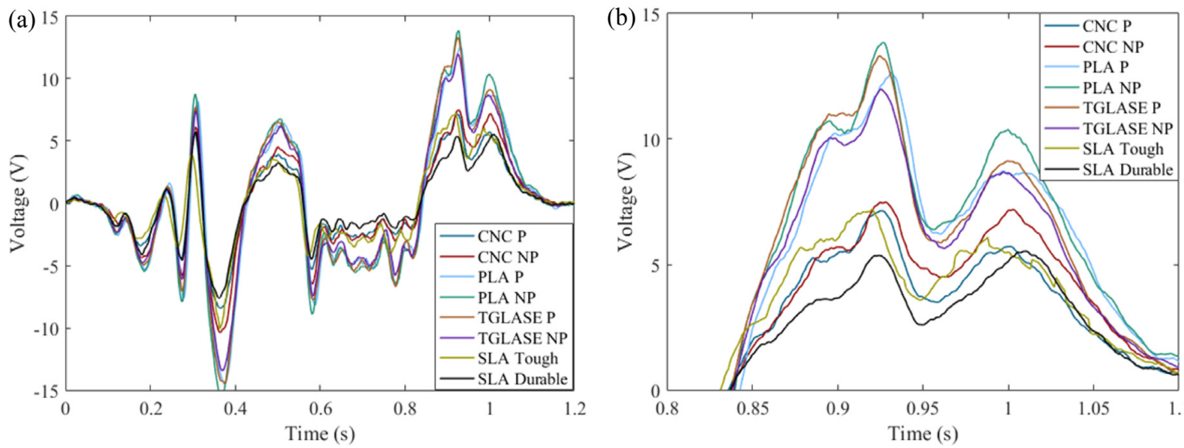

Fig. 7. Cumulative low cycle piezoelectric voltage summed for all four PZTs across (a) one loading cycle, and (b) focused view of voltage at maximum loading.

materials used in true knee implants (Sobieraj and Rimnac, 2009). It should also be noted that, at first, stiffer materials such as PLA displayed higher voltages. This behavior, however, dissipated over time, possibly with plastic deformation of the PZT pockets or, once again, settling. This points to an important consideration when performing cyclic tests on prototype implants. In general, however, once the prototypes are cycled, it seems that they display roughly the same overall voltage output, indicating no preference to any one given prototype. Investigation of the individual PZT voltage data mainly shows that load is focused on PZT 1 and that other locations, especially PZT 3, are not always under load, correlating well with the load distribution data. Investigating the load data, it is apparent that the load carried on quadrants 3 and 4 varies significantly between prototypes. This translates to larger variations in voltage on PZTs 3 and 4, which shows that, for the same experiment, different prototypes can affect individual PZT outcomes in certain areas, even if they don't affect the total voltage. Furthermore, caution should be taken when evaluating individual embedded sensor results, especially if they are in low loading areas.

3.5. Displacement

As with voltage data, displacement is evaluated for both low cycle and high cycle conditions. Recall, displacement is described as the amount of axial translation the femoral component experiences under loading. Fig. 10(a) presents the displacement results for low cycle conditions. The displacement results roughly correlate to the modulus of elasticity of the respective material. Stiffer materials such as PLA display less peak displacement while flexible materials such as CNC UHMW and t-glase display greater displacement. Outliers to this behavior are the SLA prototypes which both show higher displacement than would be expected based on their modulus. It should also be noted that polished prototypes for both FDM printed materials as well as CNC UHMW show marginally lower amounts of displacement.

High cycle displacement, much like voltage, displays interesting results when compared to low cycle displacement. Fig. 10(b) presents the displacement results for high cycle conditions. For ease of comparison, Fig. 10(c) shows the change in displacement from low cycle to high cycle conditions for all prototypes. From the results, it can be seen that both SLA prototypes display drastic decreases in displacement of around 0.15 mm (~40% reduction) after cycling, containing the lowest amount of high cycle displacement. All FDM printed prototypes decrease in displacement by approximately 0.04 mm (~10–15% reduction) after cycling. The CNC prototypes display slightly larger changes of roughly 0.05 mm (~20% reduction).

Displacement results, especially when viewed across both low cycle and high cycle conditions, play an important role in describing the kinematic behavior of the prototypes as well as supporting the voltage results discussed earlier. Once again, low cycle amplitudes of the prototypes behave roughly in accordance with the material's modulus of elasticity. This behavior changes as the prototypes are cycled, after which all prototypes display some decrease in displacement. This is supportive evidence of the strain hardening originally suggested by the voltage data. Previous work has shown that the load conditions utilized in the experiment cause higher stresses than the yield strengths listed in Table 1 (Wasielewski et al., 2004). This results in local plastic deformation in the PZT pocket area. This local plastic deformation would

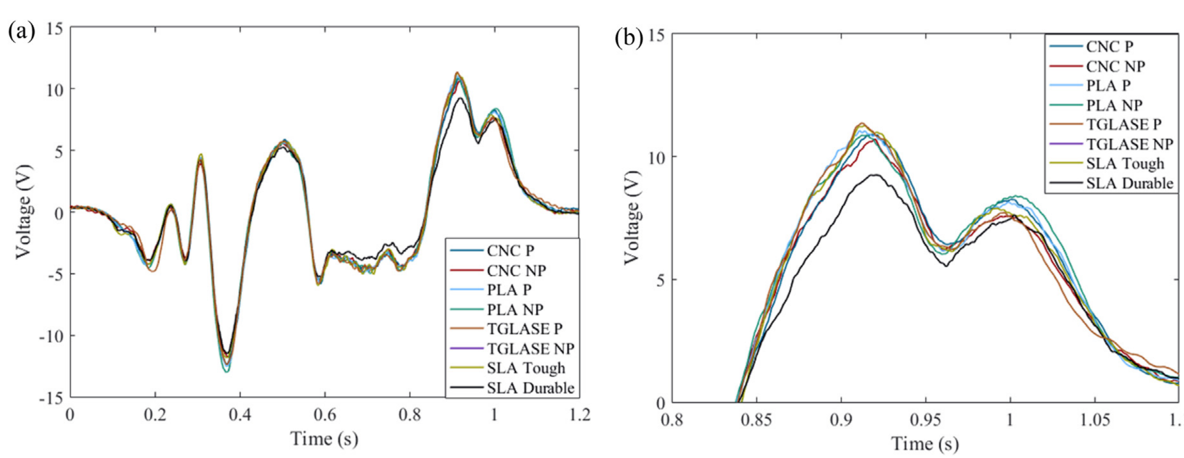

Fig. 8. Cumulative high cycle piezoelectric voltage summed for all four PZTs across (a) one loading cycle, and (b) focused view of voltage at maximum loading.

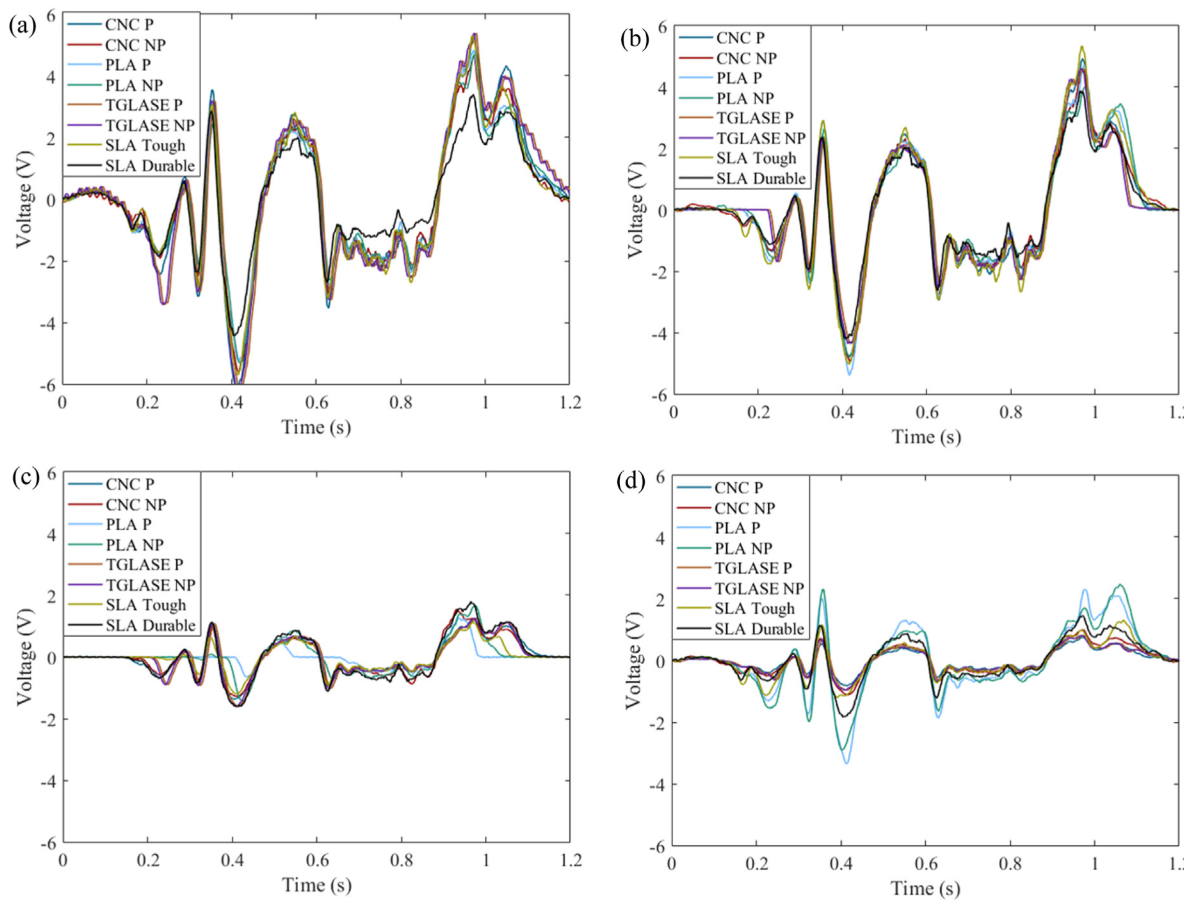

Fig. 9. Individual voltage output across one cycle in high cycle loading conditions for (a) PZT 1, (b) PZT2, (c) PZT3, and (d) PZT4.

contribute to displacement changes if work hardening occurs. It should also be noted that the softer materials, namely CNC UHMW and the SLA printed prototypes, display greater change in displacement. The SLA components may also be influenced by the layer orientation specified by the Formlabs software, Preform, which is used to define the print orientation (angle). The printed layer boundaries are angled at 45 degrees when the bearing components are set on a flat surface, meaning more of the loading stress is observed as shear. This could lead to an increase in plastic deformation or more strain hardening. This drastic change in kinematic behavior could prove problematic, depending on the desired study.

3.6. Final discussion

The results of this study have provided some general guidelines for the application of the various prototypes investigated herein and when they are optimal for use in biomechanical experimentation. Each of the eight prototypes has their own strengths and weaknesses. Though potentially inadequate for research use due to their orthotropic material properties and rough surfaces, FDM printed prototypes provide a fast and cheap method for developing surrogate implants for quick testing purposes. SLA printed prototypes, on the other hand, trade the quick fabrication times of FDM printing for high quality parts that have significantly improved surface quality as well as increased isotropic material properties. However, drawbacks include a soft surface as well as dramatic changes in kinematic behavior due to cycling. Lastly, CNC machined parts allow manufacturing of materials more similar to those used in actual knee bearings. However, CNC prototypes often require polishing to remove machining marks. If not careful, this polishing can compromise the integrity of the prototype geometry in softer materials such as UHMW. Additionally, many CNC machines require direct supervision during operation while 3D printing can often be performed unsupervised. In summary, the results of this study can be used by evaluating the demands of the specific application and ensuring the strengths and weaknesses of the chosen prototype align with the needs of the study.

4. Conclusion

This work focused on the development and performance evaluation of surrogate knee bearing implants to allow in vitro experimental analysis of implantable biomedical systems, with a special focus on those including embedded sensors. To achieve this goal, 3D scans of a real total knee replacement bearing are first captured and then used to fabricate eight different prototypes, each containing four piezoelectric sensors, and each with unique material characteristics. Fabrication processes investigated include FDM and SLA additive manufacturing as well as CNC machining. In order to compare the performance of the various prototypes, experimental evaluation is first performed to measure the hardness of each fabricated material. This is followed by experimental uniaxial load testing of the surrogate bearings to determine several characteristics. First, the load distribution between the femoral and bearing components is measured and compared to the distribution measured for a real bearing. Next, the voltage generation performance of the embedded piezoelectric transducers is measured to determine the effects of different materials and manufacturing processes on the sensing ability of such embedded transducers. Finally, the displacement under typical knee loading is measured to determine the effects of the various prototypes on joint kinematics. Results of the experimental studies show that FDM prototypes are a fast and cheap solution but suffer in terms of quality, particularly in surface area. SLA trades speed for optimal surface finish and better material properties, however

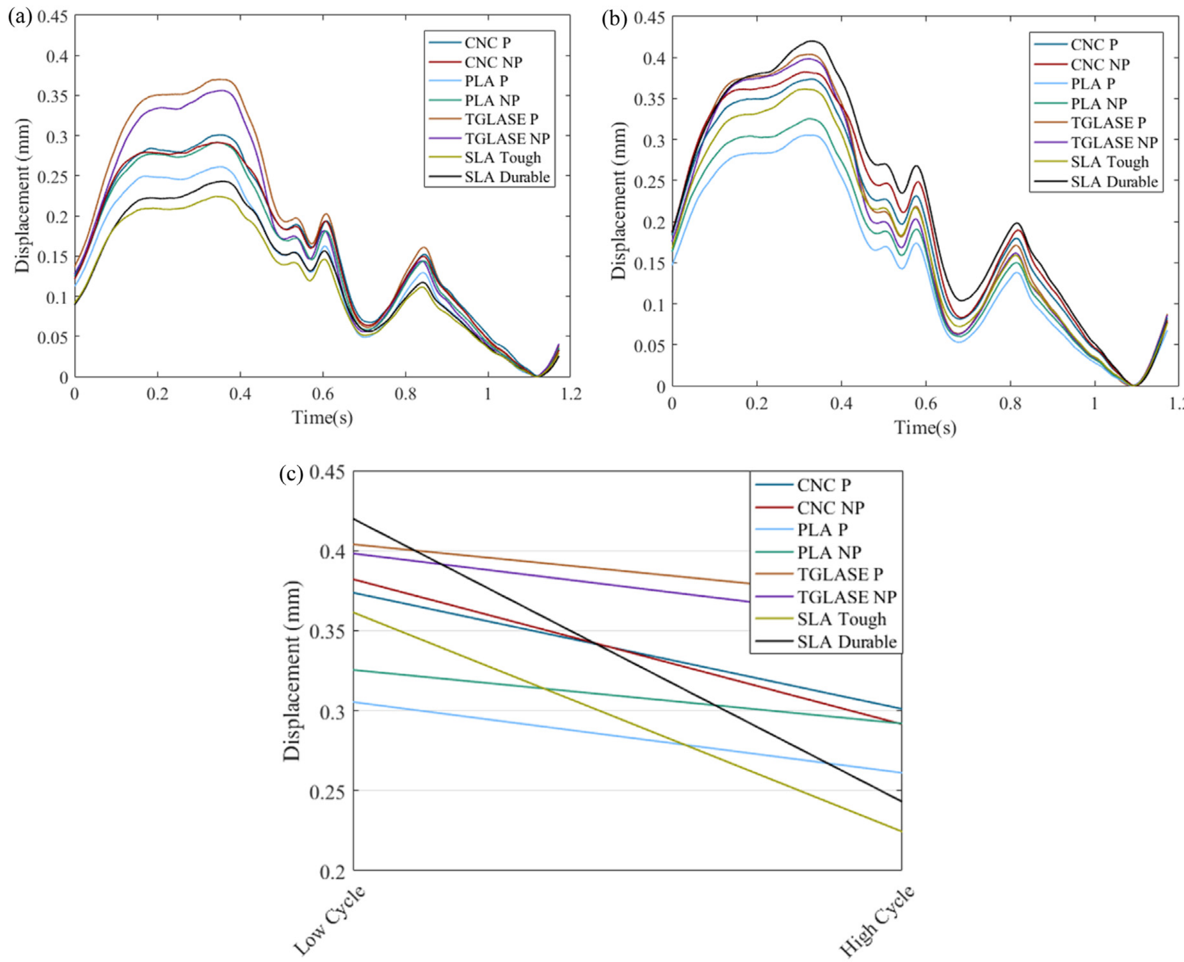

Fig. 10. Displacement at (a) low cycle, (b) high cycle, and (c) change in peak displacement from low cycle to high cycle conditions.

suffers when it comes to kinematic performance. Finally, CNC machined prototypes give the best material properties as they are made from a material that is closer to the actual bearing component material. These prototypes, however, come at an increased amount of labor and possible issues with polishing. It should also be noted that results of the experimental testing showed that the voltage generation ability and the kinematic performance both change over time with cyclic loading, thus demonstrating a settling behavior of the surrogate bearings. Of particular interest for embedded sensor applications, the voltage generation ability of all prototypes converged after many cycles. In conclusion, this study provides a foundation to aid researchers in choosing an appropriate fabrication procedure to create experimental biomedical prototypes.

Acknowledgements

Research reported in this publication was supported by the National Institute of Arthritis and Musculoskeletal and Skin Diseases of the National Institutes of Health under Award Number R15AR068663. The content is solely the responsibility of the authors and does not necessarily represent the official views of the National Institutes of Health.

References

ASTM D785-08(2015), 2015. Standard Test Method for Rockwell Hardness of Plastics and Electrical Insulating Materials. ASTM International, West Conshohocken, PA.
Bourne, R.B., et al., 2010. Patient satisfaction after total knee arthroplasty: who is satisfied and who is not? Clin. Orthop. Relat. Res. 468 (1), 57–63.
Bozic, K.J., et al., 2010. The epidemiology of revision total knee arthroplasty in the United States. Clin. Orthop. Relat. Research® 468 (1), 45–51.
Chen, H.. et al. 2007. Low power IC design of the wireless monitoring system of the orthopedic implants. In: Proceedings of the 29th IEEE Annual International Conference on the Engineering in Medicine and Biology Society, 2007. EMBS 2007.
Dixon, T., et al., 2004. Trends in hip and knee joint replacement: socioeconomic inequalities and projections of need. Ann. Rheum. Dis. 63 (7), 825–830.
Gross, B.C., et al., 2014. Evaluation of 3D Printing and Its Potential Impact on Biotechnology and the Chemical Sciences. ACS Publications.
Heinlein, B., et al., 2007. Design, calibration and pre-clinical testing of an instrumented tibial tray. J. Biomech. 40, S4–S10.
Kozanek, M., et al., 2009. Tibiofemoral kinematics and condylar motion during the stance phase of gait. J. Biomech. 42 (12), 1877–1884.
Manning, W.A., et al., 2017. Tibiofemoral forces for the native and post-arthroplasty knee: relationship to maximal laxity through a functional arc of motion. Knee Surg. Sports Traumatol. Arthrosc. 25 (6), 1669–1677.
Mannoor, M.S., et al., 2013. 3D printed bionic ears. Nano Lett. 13 (6), 2634–2639.
Murr, L.E., et al., 2012. Next generation orthopaedic implants by additive manufacturing using electron beam melting. Int. J. Biomater. 2012.
Safaei, M. and Anton, S.R., 2017. Experimental evaluation of sensing and energy harvesting behavior of implanted piezoelectric transducers in total knee replacement. In: Proceedings of the Conference on Smart Materials, Adaptive Structures and Intelligent Systems. 2017. American Society of Mechanical Engineers.
Safaei, M., Meneghini, R.M., Anton, S.R., 2017. Parametric analysis of electromechanical and fatigue performance of total knee replacement bearing with embedded piezoelectric transducers. Smart Mater. Struct. 26 (9), 094002.
Safaei, M., Meneghini, R.M., Anton, S.R., 2018a. Energy harvesting and sensing with embedded piezoelectric ceramics in knee implants. IEEE/ASME Trans. Mechatron. 23 (2), 864–874.
Safaei, M., Meneghini, R.M., Anton, S.R., 2018b. Force detection, center of pressure tracking, and energy harvesting from a piezoelectric knee implant. Smart Mater. Struct. 27 (11), 114007.
Saijo, H., et al., 2009. Maxillofacial reconstruction using custom-made artificial bones fabricated by inkjet printing technology. J. Artif. Organs 12 (3), 200–205.
Sansoni, G., Trebeschi, M., Docchio, F., 2009. State-of-the-art and applications of 3D imaging sensors in industry, cultural heritage, medicine, and criminal investigation. Sensors 9 (1), 568–601.
Sharkey, P.F., et al., 2014. Why are total knee arthroplasties failing today—has anything changed after 10 years? J. Arthroplast. 29 (9), 1774–1778.

Sobieraj, M.C., Rimnac, C.M., 2009. Ultra high molecular weight polyethylene: mechanics, morphology, and clinical behavior. J. Mech. Behav. Biomed. Mater. 2 (5), 433–443.
Verjans, M., Asseln, M., Radermacher, K., 2016. Rapid prototyping of replica knee implants for in vitro testing. Curr. Dir. Biomed. Eng. 2 (1), 553–556.
Wasielewski, R.C., Galat, D.D., Komistek, R.D., 2004. An intraoperative pressure-measuring device used in total knee arthroplasties and its kinematics correlations. Clin. Orthop. Relat. Res. 427, 171–178.
Wilson, B.E., Anton, S.R., Meneghini, R.M., 2014. Development of biomechanical knee force model for evaluation of piezoelectric sensors for in-vivo monitoring. In: Proceedings of ASME Conference on Smart Materials, Adaptive Structures and Intelligent Systems, SMASIS2014–7692 (5 pp.).